Toward Evaluation of Heat Fluxes in the Convective Boundary Layer

ZBIGNIEW SORBJAN

School of Meteorology, University of Oklahoma, Norman, Oklahoma

(Manuscript received 27 June 1994, in final form 3 October 1994)

ABSTRACT

This article demonstrates that vertical profiles of the heat flux in the convective boundary layer can be diagnosed through an integration over height of the time change rates of observed potential temperature profiles. Moreover, the basic characteristics of the convective boundary layer, such as the mixed-layer height z_i, the depth of the interfacial (entrainment) layer, and the heat flux zero-crossing height h_0 can be uniquely evaluated based on a time evolution of potential temperature profiles in the lower atmosphere.

1. Introduction

Information on sensible and latent heat fluxes within the boundary layer is essential for a general description of the dynamics in the boundary layer, as well as an input into weather prediction and climate models. Sensible and latent heat fluxes are not monitored routinely in the atmosphere. Therefore, the purpose of this paper is to demonstrate that basic characteristics of the convective boundary layer related to the vertical distribution of the fluxes can be evaluated based on a time evolution of potential temperature and mixing ratio profiles in the lower atmosphere.

2. Physical framework

Traditionally, the convective boundary is schematically divided into three layers, the surface layer, the mixed layer, and the interfacial layer (see Fig. 1). In the surface layer, the decrease of the temperature flux with height is less than 10% of its surface value (e.g., Sorbjan 1989). In the mixed layer, the potential temperature is approximately constant with height (well-mixed). Finally, in the interfacial layer above the mixed layer, there is a rapid increase (often referred to as "jump") of the potential temperature with height.

The mean thermal structure of the convective boundary layer can be described by the horizontally averaged potential temperature equation (e.g., Carlson 1973; Tennekes 1973):

$$\frac{\partial \theta}{\partial t} = -\frac{\partial H}{\partial z} + S, \tag{1}$$

where θ is the horizontally averaged potential temperature and H is the horizontally averaged temperature flux. The horizontally averaged source–sink term S includes the temperature advection term, net radiation term, and water phase changes term. All variables θ, H, and S are functions of height z and time t. In the derivation of the above equation, contributions of horizontal heat fluxes were assumed to be negligible.

We will first consider a simple case for which $S = 0$. Integrating Eq. (1) from an arbitrary height z to ∞ yields

$$H(z, t) = \int_z^\infty \frac{\partial \theta}{\partial t}(\zeta, t)d\zeta, \tag{2}$$

where $H(\infty, t) = 0$ was assumed. A similar expression was previously used by Deardorff et al. (1969) to calculate heat fluxes in their laboratory experiments. Equation (2) indicates that the temperature flux H will remain zero as long as there is no temporal changes of the potential temperature ($\partial\theta/\partial t = 0$). This often takes place in the stably stratified barotropic free atmosphere (see Fig. 1).

The two potential temperature profiles in Fig. 1 represent observations at two close instants of time, t and $t + \Delta t$. The temperature profiles intersect at two points, "1" and "2." The meaning of point 1 will be discussed later. Point 2 marks the level h, at which $\partial\theta/\partial t = 0$, and, consequently, the temperature flux vanishes. This level can be referred to as the temperature crossover height of the convective boundary layer. Since $H(\infty) = H(h) = 0$, the upper infinite bound of the integral in (2) or (3) can be replaced by h. Obviously, h varies with time.

Referring again to Fig. 1, it can be noted that the layer of air marked as $z_i < z < h$ cools with time ($\partial\theta/\partial t < 0$, for $z_i < z < h$). This cooling is due to the mixing of relatively cooler air in thermals generated near the earth's surface and relatively warmer air in

Corresponding author address: Dr. Zbigniew Sorbjan, School of Meteorology, University of Oklahoma, 401 East Boyd, Norman, OK 73019.

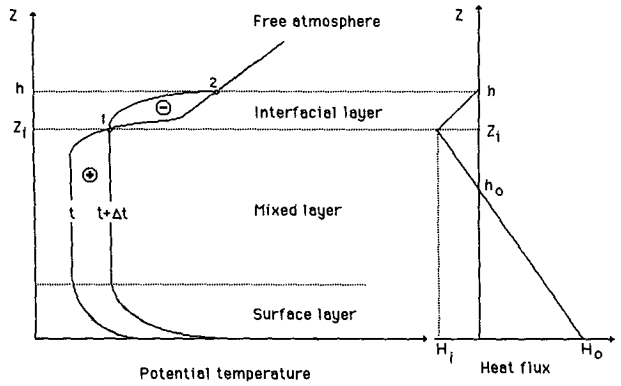

FIG. 1. A vertical structure of the convective boundary layer.

the stably stratified layer. The cooling indicates the presence of penetrative convection and the appearance of a negative sensible heat flux.

The most negative value of the temperature flux is reached at point 1. Point 1 is located at the lower intersection of the temperature profiles $\theta(t)$ and $\theta(t + \Delta t)$. Therefore, the altitude z_i of point 1 can be referred to as the temperature crossover height of the mixed layer. The most negative value of the temperature flux H_i can be obtained from (2) as

$$H_i = \int_{z_i}^{h} \frac{\partial \theta}{\partial t}\, d\zeta. \tag{3}$$

As it follows from Fig. 1 as well as Eq. (3), the value H_i is proportional to the area (marked by a minus sign) between two plotted potential temperature profiles $\Theta(t)$ and $\Theta(t + \Delta t)$ located between points 1 and 2. Lilly (1968) showed that approximately $H_i = -(\theta_2 - \theta_1)dz_i/dt$. Deardorff's (1974) LES (large-eddy simulation) experiments indicated that the accuracy of Lilly's parameterization measured as the ratio $H_i(-\Delta\theta dz_i/dt)^{-1}$ varies between 0.67 and 1.02. A similar result was obtained earlier from laboratory experiments (Deardorff et al. 1969).

A number of investigators (e.g., Tennekes 1973, Carlson 1973) have used the "zero-order slab model" with the zero depth of the interfacial layer ($h = z_i$) and with jumps in potential temperature and heat flux at the top of the mixed layer. Figure 1 and Eq. (2) indicate that even though the zero-order jump in potential temperature profile is assumed in the entraining mixed layer with $\partial z_i/dt > 0$, the zero-order jump in the heat flux will not occur [i.e., $H(z_i^+) \neq 0$].

The surface value of the temperature flux H_0 can be obtained from (2) as

$$H_0 = \int_0^{h} \frac{\partial \theta}{\partial t}\, d\zeta = \int_0^{h_0} \frac{\partial \theta}{\partial t}\, d\zeta. \tag{4}$$

Equation (4) shows that the flux H_0 can be evaluated through integration over the entire depth of the boundary layer h or through integration from the earth's surface h_0, where h_0 is the level within the mixed layer ($h_0 < z_i$) where the temperature heat flux vanishes (see Fig. 1). The level h_0 can be referred to as the heat flux zero-crossing height. In practice, integration over a more shallow domain (0–h_0) is expected to be more accurate, provided h_0 is known. Graphically, H_0 is proportional to the difference between the areas on the potential temperature plot marked by plus and minus signs in Fig. 1.

The zero-crossing height h_0 can be estimated considering the heat flux profile in Fig. 1 with two similar right-angle triangles. The first triangle is defined by its side from 0 to h_0 along the z axis, and the second one has a side from h_0 to z_i. From a simple proportion $(z_i - h_0)/(-H_i) = h_0/H_0$, one might obtain $h_0/z_i = (1 - r)^{-1}$, where $r = H_i/H_0$ is the heat flux ratio. For a typical value of $r = -0.2$, the result is $h_0/z_i = 0.83$. This value is probably slightly overestimated because the profile of the temperature flux is curved near $z = z_i$. The LES model (described in the next section) gives $h_0/z_i \approx 0.75$ for shearless convection. We adopt this value in our parameterization used below.

3. Empirical evaluation

a. LES data

Strictly speaking, Eqs. (2)–(4) define instantaneous values of heat fluxes only when the time interval Δt between the considered potential temperature profiles in Fig. 1 is infinitesimally small. In practice, however, there will be a truncation error between the value of the time derivative $\partial\theta/\partial t$ at the time instant $(t + \Delta t/2)$ in Eq. (2) and its finite-difference analog $[\theta(t + \Delta t) - \theta(t)]/\Delta t$. The truncation error will be imposed upon the errors of temperature measurements and accumulated in the process of vertical integration. All these errors might cause application of Eqs. (2)–(4) in question.

To test the feasibility of Eqs. (2)–(4), as well as the method of estimation of the temperature crossover height of the mixed layer z_i, the results generated by the LES model were first used. Generally, LES models are able to correctly simulate many features of the boundary layer as well as control individual variables in order to study their effects on the flow.

The code of the model employed in this study was written by the author and based on a subgrid parameterization and numerical scheme described by Deardorff (1973, 1974). Adams–Bashforth's scheme was employed for integration in time. The pressure equation was solved on the staggered grid (Arakawa's mesh C) by fast Fourier transform in the horizontal and three-diagonal algorithm in the vertical. The turbulence parameterization was based on the turbulent kinetic energy equation.

The model was run for 4000 s with a constant surface heat flux $H_0 = 0.06$ K m s^{-1}. The initial potential temperature profile was assumed to be as for day 33 of the

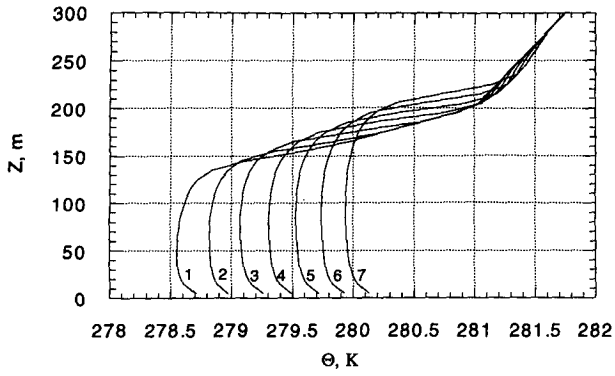

FIG. 2. Potential temperature profiles obtained from an LES model and plotted every 500 s. The first profile is obtained 1000 s after the beginning of the simulation.

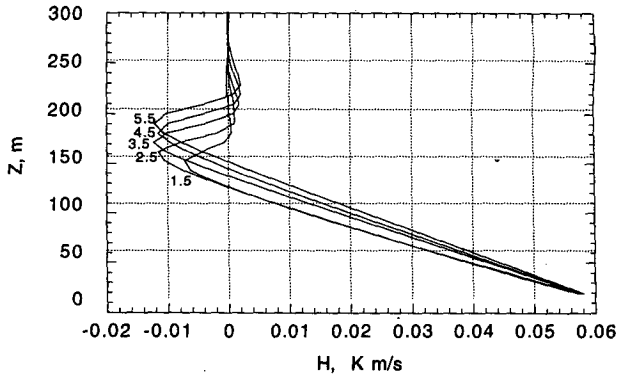

FIG. 4. Temperature flux profiles estimated from potential temperature profiles in Fig. 2. Each flux profile marked by a number $i + 0.5$ is obtained from temperature profiles marked by numbers i and $i + 1$ in Fig. 2.

Wangara experiment, at 0900 LST (Zeman and Tennekes 1977). The geostrophic wind was assumed to be zero. The roughness length was $z_0 = 0.16$ m. The integration increments were assumed to be $\Delta t = 1$ s, $\Delta x = \Delta y = 30$ m, and $\Delta z = 10$ m. The size of a domain was chosen to be quite small: $16 \times 16 \times 40$ grid points, which does not affect the presented results.

In Fig. 2, the potential temperature profiles obtained 1000 s after the beginning of the simulation are plotted every 500 s (note that the integration time increment during the simulation was $\Delta t = 1$ s). Profile 1 refers to $t = 1000$ s, and profile 7 refers to $t = 4000$ s. The corresponding temperature flux profiles are shown in Fig. 3. The first flux profile obtained at $t = 1000$ s is nonlinear. This indicates that the model at this instant of time was still in a process of transition to a steady state. All the temperature flux profiles in Fig. 3 vary from the value of 0.06 K m s^{-1} near the surface to about -0.012 (except profile 1) at the top of the mixed layer.

Figure 4 shows the temperature flux profiles estimated by using Eq. (2), with integration performed by using a simple trapezoid method. Each flux profile marked by a number $i + 0.5$ was obtained from temperature profiles marked by integer numbers i and $i + 1$ in Fig. 2 and is representative for an instant $(t_i + t_{i+1})/2$. Each flux profile in Fig. 3 represents an instant t_i. Therefore, there is no exact time correspondence between profiles in Figs. 3 and 4. Nevertheless, all the retrieved flux profiles in Fig. 4 vary as expected from the assumed value of 0.06 K m s^{-1} near the surface to about -0.012 K m s^{-1} (except profile 1) at the top of the mixed layer.

In Fig. 5, the flux H_i at the top of the mixed layer obtained from the LES model is compared with the values retrieved by using Eq. (3) and the temperature profiles in Fig. 2. The retrieved values of the flux are representative for instants $(t_i + t_{i+1})/2$. The figure shows a very good agreement between the model's direct results and the values estimated from temperature profiles.

Figure 6 depicts the time variations of the mixed-layer heights z_i. The continuous line represents z_i cal-

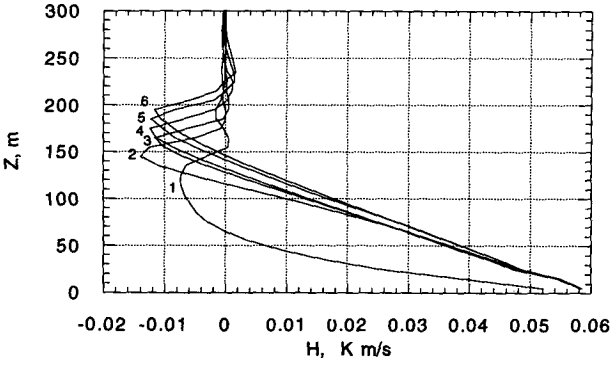

FIG. 3. Temperature flux profiles obtained from an LES model and plotted every 500 s. The first profile is obtained 1000 s after the beginning of the simulation.

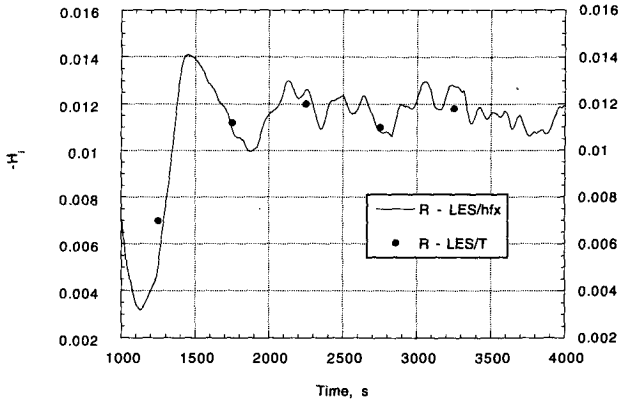

FIG. 5. The temperature fluxes at the top of the mixed layer obtained directly from an LES model (continuous line) and estimated from temperature profiles in Fig. 2 (dots).

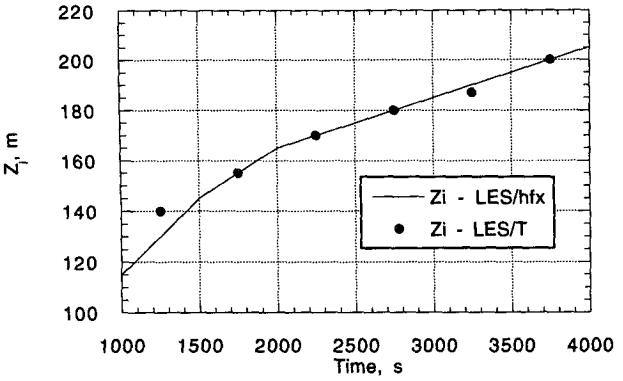

FIG. 6. The mixed-layer heights obtained directly from an LES model (continuous line) and estimated from temperature profiles in Fig. 2 (dots).

culated as the height of the most negative temperature fluxes during LES. The dots in the figure represent values of the temperature crossover height of the mixed layer z_i estimated graphically by using temperature profiles in Fig. 2. The estimated values of z_i are representative for instants $(t_i + t_{i+1})/2$. A good agreement is obtained except for the first point in the interval 1000–1500 s.

Equation (4) implies a simple parameterization that relates the surface potential temperature flux H_0, the mixed-layer height z_i, and the time change rate of the potential temperature $\Delta\theta/\Delta t$:

$$H_0 \approx \frac{h_0 \Delta\theta}{\Delta t} = 0.75 \frac{z_i \Delta\theta}{\Delta t}, \qquad (5)$$

where $\Delta\theta$ is the time change of the horizontally averaged potential temperature at the reference level, for instance, at the surface. In practice, z_i can be easier estimated than h_0.

The validity of the above parameterization can be examined using data plotted in Fig. 2. The results are summarized in Table 1. The last row presents the calculated surface fluxes H_0 for each pair of temperature profiles, i and $i + 1$, indicated in the first row. As mentioned before, the temperature profiles in Fig. 2 were obtained for $H_0 = 0.06$ K m s^{-1}. The mean of the six retrieved values is 0.059 K m s^{-1}, which gives a remarkably small average relative error for such a crude parameterization.

The expression (5) can be compared with the standard bulk parameterization

$$H_0 = C_H U_r(\Theta_2 - \Theta_1), \qquad (6)$$

where C_H is a parameter dependent on stability and roughness, U_r is the reference wind speed, and Θ_2 and Θ_1 are temperatures at two reference levels (e.g., Sorbjan 1989). It is obvious that whenever the wind speed U_r approaches 0, this parameterization fails (e.g., Stull 1994). Therefore, an approach based on Eq. (5) seems

TABLE 1. The height of the mixed layer z_i, the potential temperature change rate $\Delta\theta$, and the surface heat flux calculated from Eq. (5) for temperature profiles in Fig. 2

Profiles	1–2	2–3	3–4	4–5	5–6	6–7
Z_i (m)	140	155	170	180	185	200
$\Delta\theta$ (K)	0.3	0.27	0.23	0.2	0.2	0.2
H_o (K m s^{-1})	0.063	0.063	0.059	0.054	0.055	0.060

to be more appropriate with respect to the bulk parameterizations of Eq. (6) in wind-free convective conditions.

Equation (5) is fitted for estimation of the heat fluxes from remote sensing data (satellites, radars). Satellites enable estimation of the surface temperatures and their temporal changes in cloudless conditions. Even though errors in satellite measurements at the surface temperatures are high (4–5 K), they are highly correlated in time so the estimate of the temporal temperature change $\Delta\theta$ is quite accurate (R. Rabin 1994, personal communication). Values of z_i cannot be obtained from satellite data alone and remain to be evaluated from radar or radiosonde measurements.

b. *The Wangara data*

For further empirical examination, the "real atmosphere" radiosonde dataset was used from day 33 of a well-documented Australian experiment, "Wangara" (Clarke et al. 1971). Day 33 can be characterized as a clear-air convective regime with weak winds (2–3 m s^{-1}) and very little thermal advection.

The Wangara radiosonde profiles of the potential temperature at 0900, 1200, and 1500 are presented in Fig. 7. Figure 8 shows the corresponding retrieved temperature fluxes by using Eq. 2. The obtained values of the temperature flux at the top of the mixed layer are about 0.02 K m s^{-1} in both cases, 0900–1200 and 1200–1500. The surface temperature fluxes are in the range 0.15–0.17 K m s^{-1}. These results can be com-

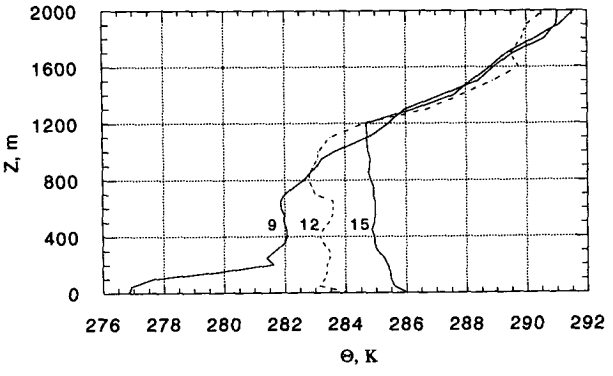

FIG. 7. Potential temperature profiles observed during day 33 of the Wangara experiment.

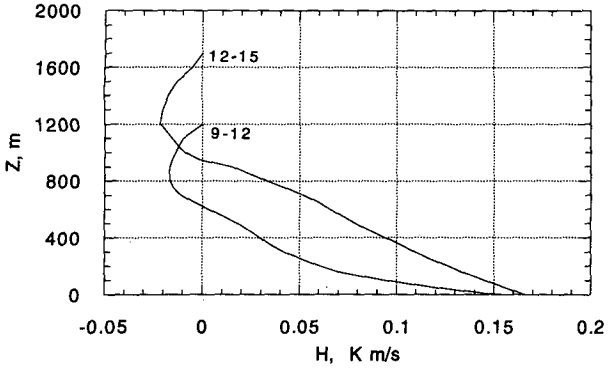

FIG. 8. Temperature flux profiles estimated from potential temperature profiles in Fig. 7.

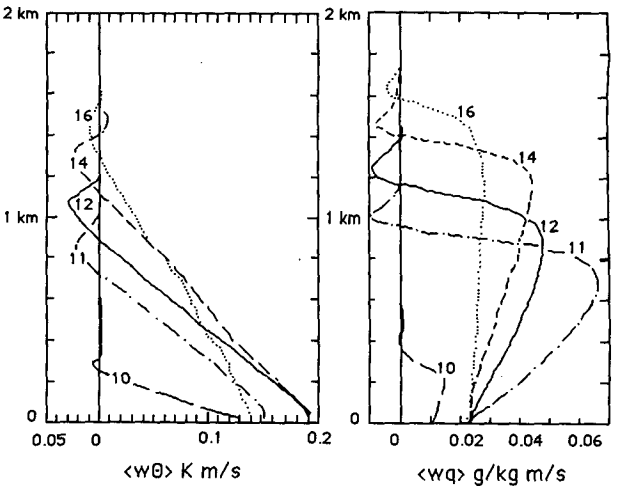

FIG. 9. Temperature and humidity flux profiles calculated from the LES model (Deardorff 1974) for day 33 of the Wangara experiment.

pared with Deardorff's (1974) LES calculations shown in Fig. 9a. In agreement with Fig. 8, Deardorff's LES values of the temperature flux at the top of the mixed layer are about 0.02 K m s^{-1} (after 1000). At the surface, the values of the temperature flux vary from about 0.13 K m s^{-1} to about 0.20 K m s^{-1}.

Estimates of the mixed-layer height z_i are shown in Fig. 10. The continuous line in the figure represents values of z_i from Deardorff's LES model, calculated as the height of the most negative temperature fluxes. The broken line represents values of z_i estimated from the mean temperature profiles calculated from Deardorff's LES model. Finally, the dots in the figure were obtained by using the observed temperature profiles in Fig. 7. The agreement for time instants after 1000 is quite good.

The validity of Eq. (5) was additionally examined by using the Wangara profiles in Fig. 7. For z_i = 1200 m and $\Delta\theta$ = 2.3 K at the surface, in the second time interval (1200–1500) the surface heat flux was H_0 = 0.19 K m s^{-1}. This value agrees with Deardorff's calculations shown in Fig. 9. Equation (5) should not be applied to the first interval (0900–1200) because the 0900 profile is stable in the surface layer.

4. Further discussion

a. *Humidity field in the cloud-free boundary layer*

The humidity field in the boundary layer can be described by a scalar equation analogous to (2):

$$\frac{\partial q}{\partial t} = -\frac{\partial Q}{\partial z} + S_q, \qquad (7)$$

where q is the horizontally averaged mixing ratio, Q is the horizontally averaged moisture flux, and S_q is the horizontally averaged source–sink term, including the moisture advection term and the water-phase changes term (condensation/evaporation).

Similarity between (1) and (2) raises a question if moisture fluxes could also be retrieved in an analogous way as the temperature field. To test this issue we considered Wangara radiosonde profiles of the specific humidity at 0900, 1200, and 1500 as shown in Fig. 11. Based on these humidity profiles, the moisture fluxes were estimated from an analog of Eq. 2 (assuming S_q = 0). The obtained fluxes are presented in Fig. 12.

The obtained surface values of the humidity flux are −0.005 g kg^{-1} m s^{-1} in the first time interval (0900–1200) and 0.0185 g kg^{-1} m s^{-1} in the second time interval (1200–1500). These results can be compared with Deardorff's calculations shown in Fig. 9b. The negative peaks in humidity fluxes in Fig. 9 at the top of the mixed layer are spurious (Deardorff 1974). The fact that humidity fluxes increase with height in the lower portion of the mixed layer indicates that humidity decreases with time in this region. This can be confirmed in Fig. 11.

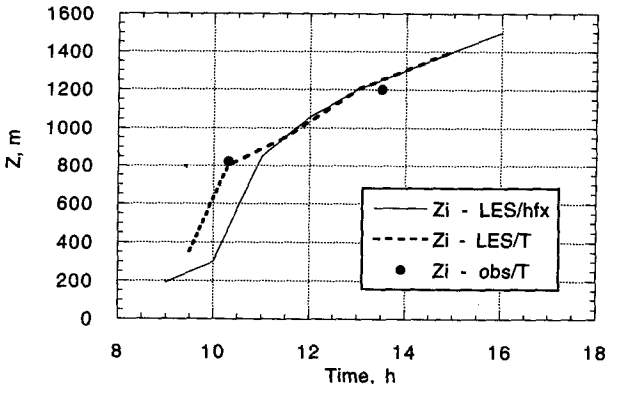

FIG. 10. The mixed-layer height history for day 33 of the Wangara experiment based on Deardorff's (1974) LES heat profiles in Fig. 9 (continuous line), estimated based on Deardorff's (1974) LES temperature profiles (dotted line), and estimated based on observed temperature profiles in Fig. 8 (dots).

The humidity flux near the surface in Fig. 12 for the time interval (1000–1200) is underestimated and has a negative sign. The second flux profile has a proper value of about 0.02 g kg^{-1} m s^{-1} near the surface. These results seem to be influenced by a likely erroneous peak in mixing ratio profile at $z = 1000$ m and at $t = 1200$.

b. *Cloud-topped boundary layer*

The presence of clouds in the boundary layer leads to considerable complications due to the role played by radiative fluxes and phase changes (e.g., Garratt, 1992). When the top of the boundary layer is covered by clouds, the water phase changes term is nonzero. To eliminate this term from Eq. (1) and (7), the equation for the equivalent potential temperature $\theta_e = \theta + (\theta/T)(L/c_p q)$ can be derived (e.g., Deardorff 1976). In the absence of precipitation, with an assumption that $\theta/T \approx 1$ and $S_a = 0$ (no heat advection), this equation has the following form:

$$\frac{\partial \theta_e}{\partial t} = -\frac{\partial H_e + R}{\partial z}, \tag{8}$$

where $H_e = H + L/c_p Q$ is the flux of the equivalent potential temperature and R is the net radiative flux.

Integrating Eq. (8) from an arbitrary height z to h yields

$$H_e(z) + R(z) - R(h) = \int_z^h \frac{\partial \theta_e}{\partial t}\, d\zeta, \tag{9}$$

where h is defined as before. The obtained equation has an analogous interpretation as Eq. (3). As in the case of the potential temperature in the cloud-free boundary layer in Fig. 1, the two equivalent potential temperature profiles $\theta_e(t)$ and $\theta_e(t + \Delta t)$ are also expected to intersect at two points. The upper point will mark the level h above the cloud, at which the total flux $H_e(z) + R(z) - R(h)$ vanishes. The most negative value of the total flux $H_e(z) + R(z) - R(h)$ will be reached at the point located at the lower intersection

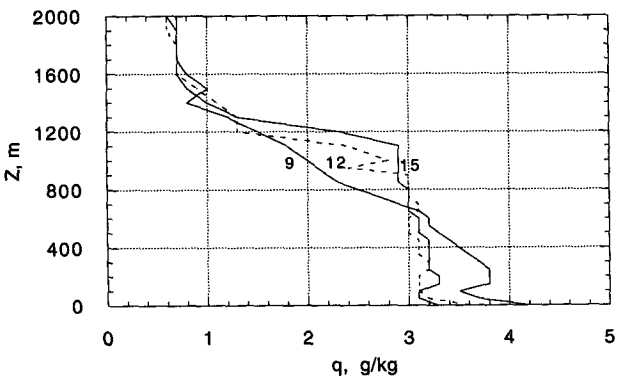

FIG. 11. Mixing ratio profiles obtained during day 33 of the Wangara experiment.

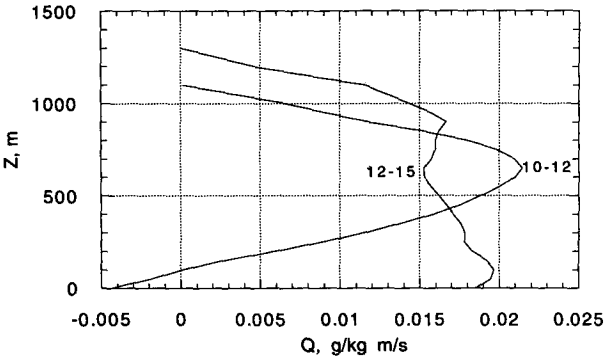

FIG. 12. Humidity flux profiles estimated from profiles in Fig. 11.

of the temperature profiles $\theta_e(t)$ and $\theta_e(t + \Delta t)$ (e.g., Sun, 1993). Unless additional information on radiative fluxes is provided (e.g., from satellite and surface observations), it is impossible to partition the total flux $H_e(z) + R(z) - R(h)$ into the turbulent and radiative fluxes.

c. *Advection*

So far the presented discussion has been limited to cases with no horizontal advection. Such cases are easily distinguishable by the fact that the potential temperature profiles (as well as the mixing ratio profiles) do not vary significantly with time above the mixed layer. In some situations, however, the advective term in Eq. (1) [and also in (7) and (8)] might be substantial and has to be accounted for in order to obtain accurate estimates of fluxes in the boundary layer. This requires measurements of temperature and mixing ratio profiles in at least three locations. In some cases the effect of vertical motions (subsidence) can also be significant. Unfortunately, its contribution is very difficult to measure.

Equation (2) indicates that neglecting the cold advection of air ($S_a < 0$) will lead to underestimation of the boundary layer fluxes. On the other hand, neglecting the warm advection ($S_a > 0$) will lead to overestimation of the boundary layer fluxes. For example, if the temperature change is uniform in the layer of 600 m and equal to 10 K per 6 h, the error in the value of the surface temperature flux due to neglecting of the advective effects is about 0.3 K m s^{-1}.

Acknowledgments. Conversations with Dr. Richard Doviak, Dr. Chin-Ho Moeng, and Donald Lenschow regarding this work are highly appreciated. This research was sponsored by NSF Grant ATM 9217028.

REFERENCES

Carlson, D. J., 1973: The development of a dry, inversion-capped, convectively unstable boundary layer. *Quart. J. Roy. Meteor. Soc.*, **99**, 450–467.

Clarke, R. H., A. J. Dyer, R. R. Brook, D. G. Reid, and A. J. Troup, 1971: The Wangara Experiment: Boundary layer data. CSIRO Div. Meteor. Phys., Tech. Pap. No. 19, 350 pp.

Deardorff, J. W., 1973: Three-dimensional numerical modeling of the planetary boundary layer. *Workshop of Micrometeorology,* D. A. Haugen, Ed., Amer. Meteor. Soc.

——, 1974: Three-dimensional numerical study of the height and mean structure of a heated planetary boundary layer. *Bound.-Layer Meteor.,* **7,** 81–106.

——, 1976: On the entrainment rate of a stratocumulus-topped mixed layer. *Quart. J. Roy. Meteor. Soc.,* **102,** 563–582.

——, G. E. Willis, and D. K. Lilly, 1969: Laboratory investigation of non-steady penetrative convection. *J. Fluid. Mech.,* **35,** 7–31.

Garratt, J. R., 1992: *The Atmospheric Boundary Layer.* Cambridge University Press, 316 pp.

Sorbjan, Z., 1989: *Structure of the Atmospheric Boundary Layer.* Prentice-Hall.

Stull, R., 1994: A convective transport theory for surface fluxes. *J. Atmos. Sci.,* **51,** 3–22.

Sun, W.-Y., 1993: Numerical simulation of a planetary boundary layer. Part II: Cloudy case. *Beitr. Phys. Atmos.,* **66,** 17–29.

Tennekes, H., 1973: A model for the dynamics of the inversion above a convective boundary layer. *J. Atmos. Sci.,* **30,** 558–567.

Zeman, O., and H. Tennekes, 1977: Parameterization of the turbulent energy budget at the top of the daytime atmospheric boundary layer. *J. Atmos. Sci.,* **34,** 111–123.